WARSAW UNIVERSITY OF TECHNOLOGY Index 351733
FACULTY OF CIVIL ENGINEERING
COMMITTEE FOR CIVIL AND WATER ENGINEERING
POLISH ACADEMY OF SCIENCES ISSN 1230-2945

DOI: 10.24425/ace.2025.154117
ARCHIVES OF CIVIL ENGINEERING
Vol. LXXI ISSUE 2 2025

pp. 209 –224

Research paper

The influence of the accuracy of reproducing the uniaxial tensile test of mild steel in the H–M plasticity model on the behaviour of a perforated thin walled shell subjected to compression

Andrzej Piotrowski[1], Marcin Gajewski[2], Stanisław Jemioło[3], Cezary Ajdukiewicz[4]

Abstract: The article describes the impact of modeling the plasticity constitutive relationship on the buckling of a short section of a perforated thin-walled steel bar with an open cross-section (modeled as a perforated shell) subjected to compression, being one of the elements of a high-storage system. Numerical calculations were performed in the ABAQUS/Standard program with application of the elasto-plasticity theory of large deformations with additive decomposition of the logarithmic strain tensor and taking into account the nonlinear isotropic or kinematic strain hardening models. The isotropic nature of the material was considered and the plastic flow law associated with the Huber-Mises plasticity condition was assumed. In the elasticity range, linear characteristics of the material was assumed, while in the plasticity range, the shape of the uniaxial strain hardening curve was described as piecewise linear approximation of plastic strain-stress graphs obtained from uniaxial tensile tests. The 24 sets of material data obtained on the basis of experimental tests were analyzed and the influence of differences in the values of material parameters were described (in tests carried out on samples cut from the modeled bars, large differences were found in the values of material parameters and the shape of uniaxial tension graphs). Also the accuracy of strain hardening modeling (the number of sections assumed in the model piecewise linear) on the calculated bearing capacity force value was considered and evaluated.

Keywords: elasto-plasticity, FEM, limit load, perforated bars, stability, thin-walled bars

[1]PhD, Warsaw University of Technology, Faculty of Civil Engineering, Al. Armii Ludowej 16, 00-637 Warsaw, Poland, e-mail: andrzej.piotrowski@pw.edu.pl, ORCID: 0000-0003-4407-7344
[2]DSc, Warsaw University of Technology, Faculty of Civil Engineering, Al. Armii Ludowej 16, 00-637 Warsaw, Poland, e-mail: marcin.gajewski@pw.edu.pl, ORCID: 0000-0002-3171-8504
[3]Prof, Warsaw University of Technology, Faculty of Civil Engineering, Al. Armii Ludowej 16, 00-637 Warsaw, Poland, e-mail: stanislaw.jemiolo@pw.edu.pl, ORCID: 0000-0001-5285-7776
[4]PhD, Warsaw University of Technology, Faculty of Civil Engineering, Al. Armii Ludowej 16, 00-637 Warsaw, Poland, e-mail: cezary.ajdukiewicz@pw.edu.pl, ORCID: 0000-0003-2315-796X

1. Introduction

The issues of global and local stability of thin-walled bars or shell elements are very important from the engineering point of view [1, 2]. Solutions that use thin-walled elements (e.g. thin-walled bars) or thin-walled structures are justified for both economic and strength reasons. The theory of thin-walled bars is quite well developed, and the solutions to stability problems take well into account the nature of the expected solutions [3, 4], i.e. flexural buckling, flexural-torsion buckling, etc. However, these solutions are insufficient for elements with relatively small slenderness [5], because then the phenomenon of local loss of stability of the cross-section walls in the elastic range or the phenomenon of elasto-plastic buckling is highlighted [6, 7]. It can be concluded that in such situations the analyzed compression bar should be defined as a shell [8–11], and constitutive modeling should take into account not only elastic but also plastic material properties [8–10, 12–14].

The element of the high storage system analyzed in this work is a thin-walled steel perforated bar [15–17] (technological/assembly holes), which introduces significant localization of stress and strain fields (sharp corners of holes) and even forces the application of the elasto-plasticity theory. By conducting experimental tests on the compression of this type of elements [6, 10, 11, 18–21], it can be noticed that after exceeding the critical force (bearing capacity), the values of displacements and local rotations in the loaded element increase rapidly, which in turn leads to the need to apply the theory of large deformations.

The application of the theory of elasto-plasticity of large deformations and the treatment of a thin-walled perforated bar as a perforated shell means the need to conduct numerical calculations – the ABAQUS [22] program was used in this work. The theory of elasto-plasticity of large deformations available in the program for isotropic metals with additive decomposition of the logarithmic strain tensor, flow law associated with the Huber–Mises plasticity condition and nonlinear isotropic or kinematic strain hardening were used. Among the strain hardening options available in the program, an uniaxial, piecewise linear model was selected, based on data from a uniaxial tensile test. In the elastic range, Hooke's linear relationship was adopted.

In the conducted experimental compression tests of the described bars [6, 10, 11, 20] and especially in uniaxial tensile tests of samples cut from them, large differences were noticed between the results obtained for samples obtained from individual, theoretically identical, elements.

The aim of this article is to assess the impact of the observed differences in steel properties and the method of describing its elastic-plastic properties on the obtained critical forces (interpreted as forces corresponding to the ultimate compressive load capacity) in the static compression task of a selected thin-walled profile. In accordance with the standard for steel structures [23, 24] the simplified modeling of material properties adopted in this article is allowed, and thanks to the results presented below, it is possible to qualitatively and quantitatively assess the impact of these simplifications on the predictions of the computational model.

2. Description of the analysed problem

Perforated shells corresponding to short sections of a thin-walled steel bars constituting an element of a high storage system are analyzed. The cross-section of these bars is open and resembles a rectangular Greek letter Ω without lower horizontal lines and slightly dented at the top. This type of the cross-section was obtained by cold bending of steel sheets [25]. Due to the manufacturer's failure to maintain a high quality of the product, the steel properties vary significantly between individual elements [11]. The bars are equipped with 4 rows of symmetrically arranged holes running along their entire length and used to attach other storage elements. The rows on the open side of the cross-section (in other words, close to its free ends) consist of 6.8 mm diameter circular holes, while the rows on the closed side of the cross-section (on its spine) consist of alternating circular and trapezoidal holes with a maximum width of approximately 16 mm. The difference in shape results from different applications within the storage system – smaller holes are used to attach trusses, and larger ones are used to attach beams.

Sections of lengths 50, 100, 150, 200, 250, 300, 400 and 500 mm were cut from the described rods and prepared for experimental tests [6, 18, 19, 26], and such lengths were also assumed in the numerical calculations described in this article. The geometry of the analyzed shells is shown in Fig. 1.

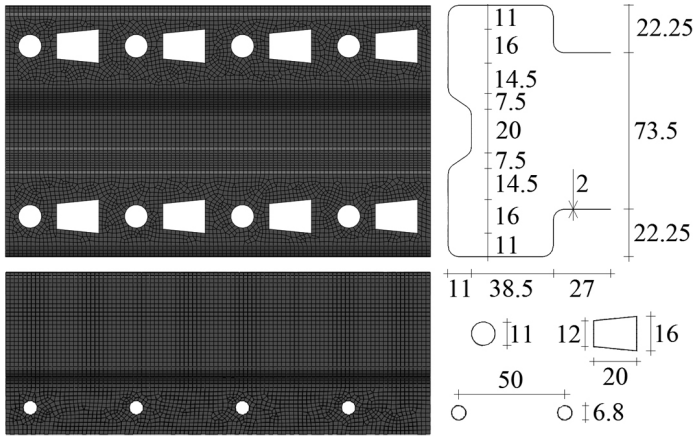

Fig. 1. Dimensions and an exemplary mesh for a two hundred millimeter shell (in mm)

3. Material modelling

3.1. Constitutive model

The issue was formulated within the framework of the elastic-plastic theory of large deformations with additive decomposition of the strain tensor $\boldsymbol{\varepsilon} = \mathbf{V}$ into parts: plastic $\boldsymbol{\varepsilon}_p = \ln \mathbf{V}_p$ and elastic $\boldsymbol{\varepsilon}_e = \ln \mathbf{V}_e$, which is available in the ABAQUS program, cf. [27–29].

We determine the elastic part of strains based on Hooke's relation for isotropic materials:

$$\boldsymbol{\varepsilon}_e = -\frac{\nu}{E}(\operatorname{tr}\boldsymbol{\sigma})\mathbf{I} + \frac{1+\nu}{\mathrm{E}}\boldsymbol{\sigma} \tag{3.1}$$

where E is Young's modulus and ν is Poisson's ratio. However, it is not possible to determine a direct relationship to the plastic part in the case of the plastic flow theory. Then the plastic flow function is used, which determines the plastic strain rate tensor $\dot{\boldsymbol{\varepsilon}}_p$ after the material reaches the plastic state. The relationship on the plastic part of strain postulated in the form of the flow law associated with the plasticity condition f has the form:

$$\dot{\boldsymbol{\varepsilon}}_p = \lambda \frac{\partial f}{\partial \boldsymbol{\sigma}}\bigg|_{\boldsymbol{\sigma}} = \boldsymbol{\sigma}^T, \qquad \lambda \geq 0 \tag{3.2}$$

where $f = 0$ defines the yield condition in the stress state space. For $f \leq 0$ the material is in elastic state, which corresponds to $\dot{\boldsymbol{\varepsilon}}_p = 0$ (i.e. plastic multiplier $\lambda = 0$). When the stress condition reaches the condition $f = 0$, plastic deformations occur in the body, and therefore the stress state is determined by the plasticity condition. The plastic strain rate tensor is defined according to the normal to the yield surface. In order for the surface f to uniquely define the transition to the plastic state, the function f must be a convex function in relation to σ. If short-term and rapidly changing loads are omitted, the assumption is often made that the plastic part of the strain increase is incompressible, i.e. $\operatorname{tr}\dot{\boldsymbol{\varepsilon}}_p = 0$. Therefore, in materials meeting this condition, permanent deformations are assumed to be deviatoric, which results in the function $f(\boldsymbol{\sigma})$ is not dependent on the trace of the stress tensor (cf. Huber–Mises, Coulomb–Treska and other plasticity conditions [30, 31]). To describe the plastic properties of steel, the Huber-Mises plasticity condition with isotropic, kinematic or mixed strain hardening was adopted. The Huber–Mises failure criteria equation with mixed strain hardening can be written in the following form:

$$F(\boldsymbol{\sigma}, \bar{\varepsilon}^{pl}) = f(\boldsymbol{\sigma}) - \sigma^0(\bar{\varepsilon}^{pl}) \tag{3.3}$$

The yield condition is expressed as:

$$f(\boldsymbol{\sigma}) = \sqrt{\frac{2}{3}(\mathbf{s}-\boldsymbol{\alpha})\cdot(\mathbf{s}-\boldsymbol{\alpha})} \tag{3.4}$$

where $\mathbf{s} = \boldsymbol{\sigma} - \frac{1}{3}\operatorname{tr}\boldsymbol{\sigma}$ is a deviatoric part of the stress tensor, α is the translation tensor in the deviatoric plane of the plasticity condition (in fact it is a deviator tensor, i.e.$\operatorname{tr}\boldsymbol{\alpha} = 0$), $\bar{\varepsilon}^{pl}$ stands for equivalent plastic strains, $\sigma^0(\bar{\varepsilon}^{pl})$ is a function of the stress in the uniaxial tensile test, and the dot indicates the full contraction of the tensors. Function $\sigma^0(\bar{\varepsilon}^{pl})$ can be approximated in various ways, and the impact of this approximation on the model's predictions is, among other things, the purpose of this article. Non-linear strain hardening function $\sigma^0(\bar{\varepsilon}^{pl})$ will be approximated in this work by a piecewise linear function with any number of intervals, which is one of the options available in the ABAQUS program [32].

The constitutive model should be supplemented with a kinematic equation for the tensor increment $\boldsymbol{\alpha}$, for example in the form like in [33]:

$$\dot{\boldsymbol{\alpha}} = \frac{C}{\sigma^0}(\boldsymbol{\sigma}-\boldsymbol{\alpha})\dot{\bar{\varepsilon}}^{pl} - \gamma\boldsymbol{\alpha}\dot{\bar{\varepsilon}}^{pl} \tag{3.5}$$

where C and γ are strain hardening parameters usually determined from cyclic tests. If we assume in the model $C = 0$ and $\gamma = 0$, then we obtain a model with isotropic strain hardening described by function (3.5). If, in turn, we assume $Q = 0$, then we will get a model with kinematic strain hardening [34].

3.2. Material data

A total of 24 material data sets were analyzed, including 16 material data sets generated from four different tensile tests and 8 material data sets generated from the maximum and minimum values of elastic modulus, yield stress and tensile strength calculated from thirteen different tensile tests (Table 1. It should be recalled here that for calculations using the large strains theory, it is necessary to convert engineering strains and stresses into logarithmic ones [34] and model the hardening curve in piecewise-linear form. During the tests, heterogeneity of steel and large differences in parameters between samples cut from different, assumedly identical, elements were noticed.

Table 1. Material test results on 13 samples (engineering values)

	Average value	**Standard deviation**	**Minimum value**	**Maximum value**
E [GPa]	198	25	161	235
R_H [MPa]	352	37	283	403
R_{pl} [MPa]	431	18	402	458
R_m [MPa]	511	13	486	529

Sixteen sets of data were obtained in this way: for each of the four selected samples, four sets of data were created, differing in the number and location of points approximating the stress-plastic strain curve: two precise sets, containing about 10 points, and two coarse sets, approximating the graph with a straight line; in each of these pairs, one set took the proportionality limit R_H as its starting point, and the other set took the yield stress R_{pl} as its starting point, as shown in Fig. 2 on the example of sample 1. Tensile graphs of the 4 samples used for modeling are shown in Fig. 3.

Eight data sets were created based on extreme values of elastic modulus, yield stress, and tensile strength obtained from conducting thirteen tensile tests. A linear stress-plastic strain relationship was assumed from the yield point to the tensile strength, as shown in Fig. 4.

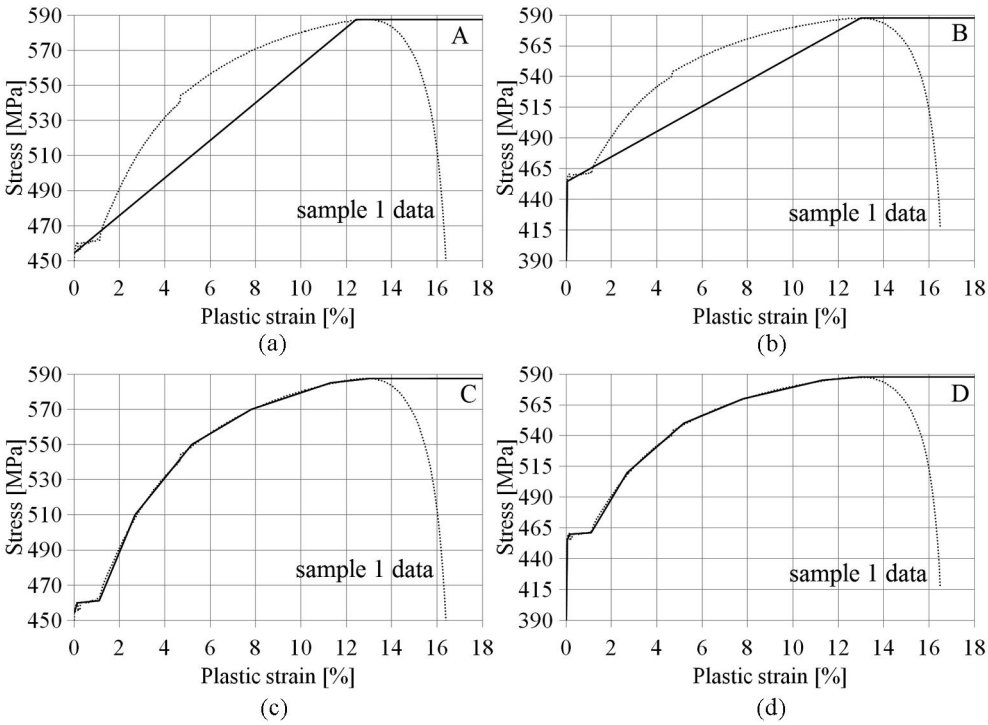

Fig. 2. True stress – plastic strain relationships for sample 1: dotted line – experimental results, solid line – relationship used for calculations; a) coarse approximation, beginning in R_{pl} (A), b) coarse approximation, beginning in R_H (B), c) fine approximation, beginning in R_{pl} (C), d) fine approximation, beginning in R_H (D)

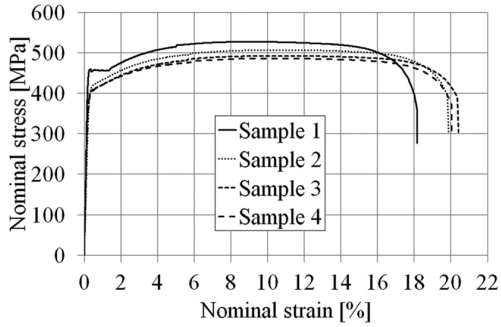

Fig. 3. Tensile graphs for samples 1–4

Each set is identified by three letters, the first of which refers to the Young's modulus, the second to the yield point, and the third to the tensile strength, with "D" meaning the maximum value and "M" the minimum. The data entered into the ABAQUS program are presented in Table 2. It was assumed that the R_m value is achieved at a plastic strain of 13%.

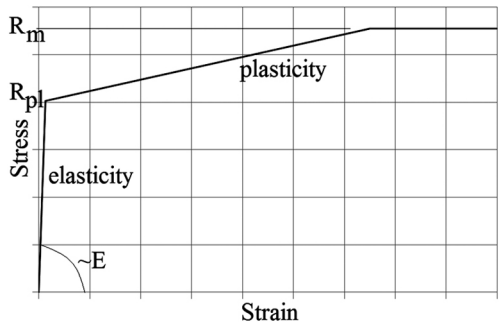

Fig. 4. Simplified material data sets generated from extremes

Table 2. Simplified material data sets according to extremes (logarithmic values)

Set	E [GPa]	R_{pl} [MPa]	R_m [MPa]
MMM	161	403	555
MMD			605
MDM		459	555
MDD			605
DMM	235	403	555
DMD			604
DDM		459	555
DDD			604

A comparison of the results for kinematic and isotropic hardening was also made. For this purpose, data for sample 1 with a simplified representation of the stress-plastic strain relationship were used (only two points were used, one corresponding to the yield point and the other to the tensile strength, in accordance with Fig. 2a). In both cases (isotropic and kinematic hardening), exactly the same points were adopted.

4. FEM modelling

Calculations were made using the ABAQUS/Standard program [35]. An incremental Newton-Raphson algorithm without stabilization was used. Automatic step division was adopted, forcing the first increment by 0.01 of the whole step length equal to unity. The calculations were carried out according to the large deformation theory (i.e. with the NLGEOM option enabled, see [27, 36]). In some cases, it was necessary to shorten the increment, use stabilization and the Riks algorithm, but in conditions where the Newton-Raphson algorithm was sufficient, the Riks algorithm gave almost identical results. Displacement boundary conditions at the compressed ends and finite elements S3 and S4R were used. These are

general-purpose shell elements (for thick and thin shells), three- and four-node respectively, suitable for use in large deformation theory calculations; four-node elements use reduced integration and hourglass control (marked R). The adopted mesh used mainly quadrangular elements, while triangular elements played an auxiliary role. An automatic mesh creation algorithm was used. After conducting a convergence analysis, it was decided to adopt a mesh with a typical element size of approximately 2 mm (approximately 4000 elements per 5 cm of shell length). An example mesh is shown in Fig. 1. 192 tasks were solved corresponding to all possible combinations of the length and material data given above for isotropic hardening and 8 tasks for kinematic hardening – a total of 200 tasks. All calculations were performed with full end restraint and no geometrical imperfections.

5. Presentation of FEM results and their analysis

The results obtained on the basis of data defined according to Fig. 2 are shown in Figs. 5 and 6, with Fig. 5 showing exemplary equilibrium paths, and Fig. 6 showing graphs presenting the dependence of the critical force on length. As you can easily see, on the basis of the data from sample 1, significantly higher critical force values were obtained than from the other samples. Taking the proportionality limit instead of the yield point as the beginning of yielding allows

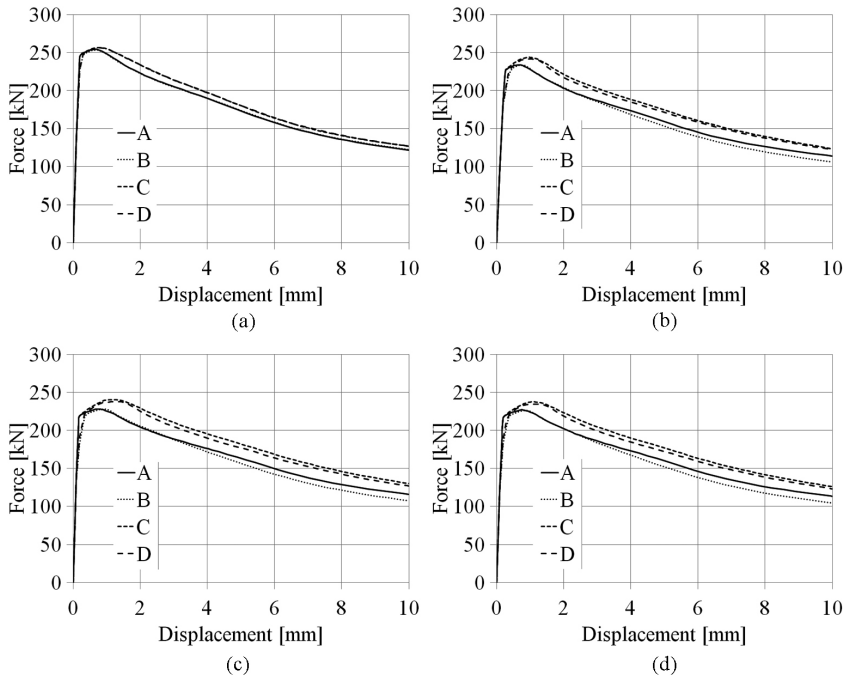

Fig. 5. Equilibrium paths for a 100 mm long shell – 16 sets according to Fig. 2; a) sample 1, b) sample 2, c) sample 3, d) sample 4

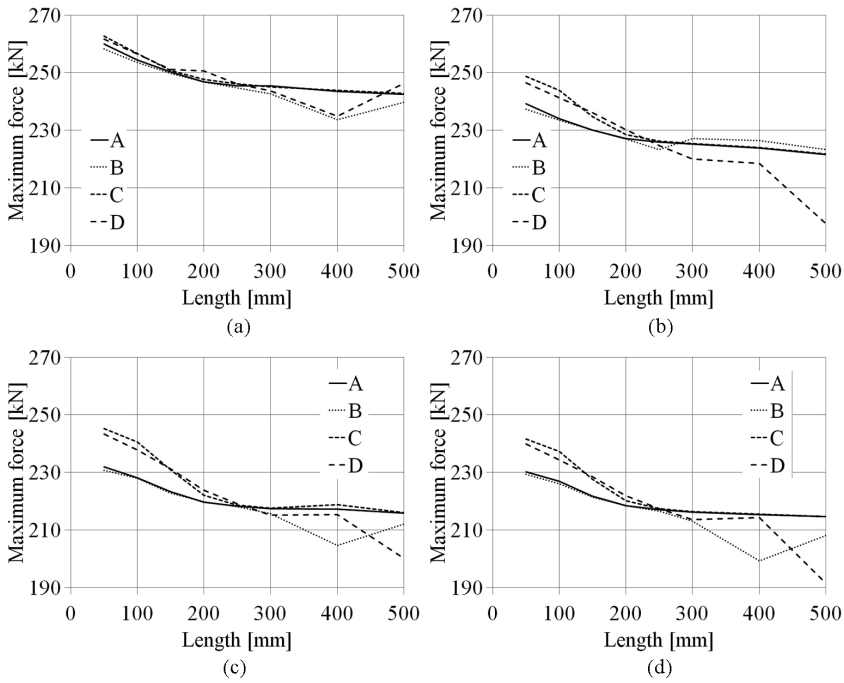

Fig. 6. Critical force-length relations – 16 sets according to Fig. 2; a) sample 1, b) sample 2, c) sample 3, d) sample 4

for obtaining a smoother curve at the moment of buckling, closer to the experimental results. Differences between the results obtained for precisely and roughly reproduced stress-plastic strain curves affect the value of the critical force (impact of several percent, for more accurate mapping results closer to those obtained in the experiment [6, 10, 11, 18–21, 26], are also noticeable in the post-critical phase, with more accurate mapping giving higher force values, and less accurate – lower ones. The value of the elastic modulus is, of course, most important in the linear phase of shell compression. It should be noted here that some of the tasks could not be calculated with the adopted algorithm parameters and it was necessary to modify the minimum increment length, introduce stabilization or use the Riks algorithm. Sometimes this resulted in a change in the form of buckling (Fig. 7) and outlier results of the critical force (Fig. 6), which is possible from the theoretical point of view of the nonlinear theory of large deformations [27], as there is no unambiguity in this theory solutions to boundary problems even in range of the elastic properties of the material.

The results obtained on the basis of the data from Table 2 are shown in Figs. 8 and 9, with exemplary equilibrium paths in Fig. 8 and graphs showing the dependence of the critical force on length in Fig. 9. As you can easily see, the value of the yield point has the greatest impact on the obtained results, the modulus of elasticity affects mainly (but not only) the linear elastic range, and the strength affects the post-critical course. The reason why one of the results in Fig. 9a is outlier is the change in the form of buckling, analogous to that shown in Fig. 7 in the context of Fig. 6.

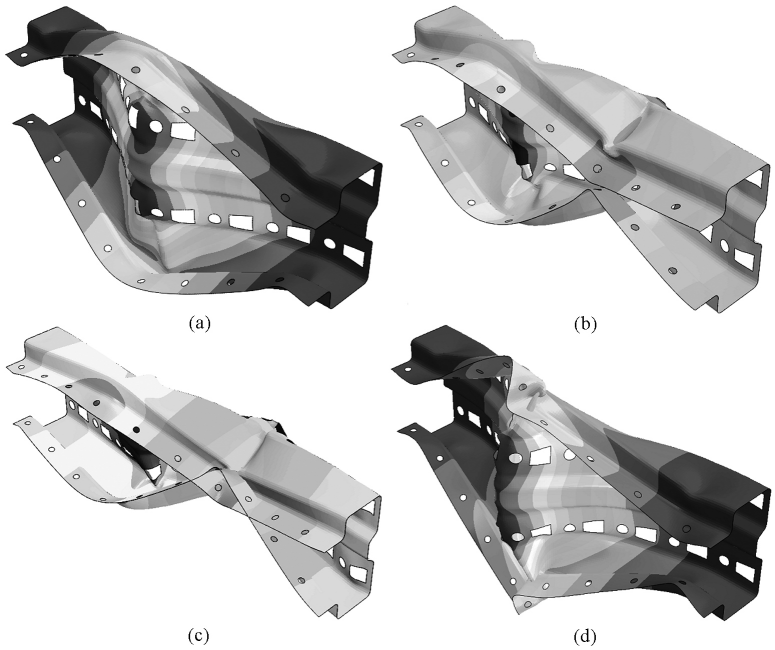

Fig. 7. Change in the form of buckling for data according to sample 3 (Fig. 6c); a) 400 mm shell, modeling B, b) 400 mm shell, modeling D, c) 500 mm shell, modeling B, d) 500 mm shell, modeling D

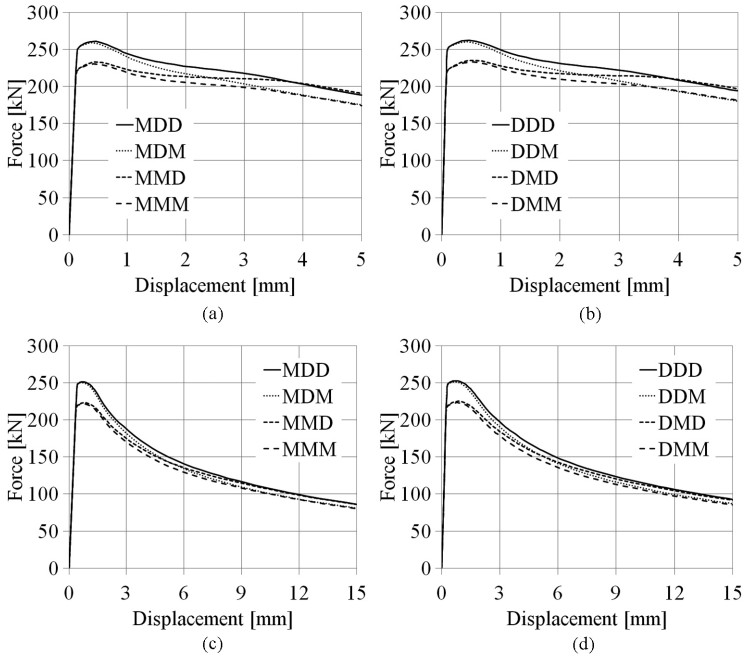

Fig. 8. Equilibrium paths – 8 sets according to Table 2; a), b) 50 mm, c), d) 150 mm

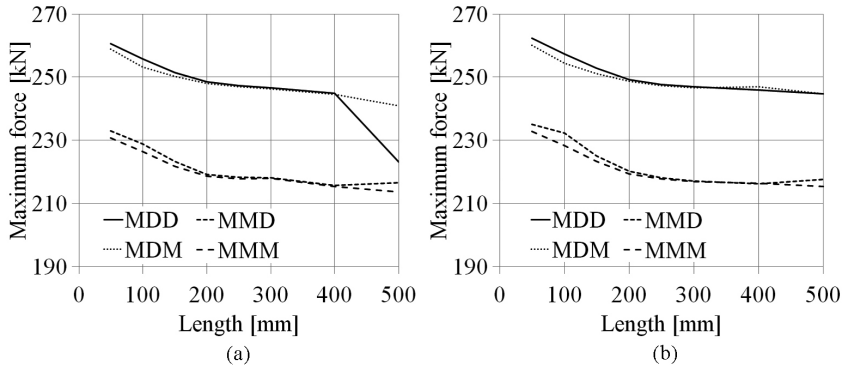

Fig. 9. Critical force-length relations – 8 sets according to Table 2

A comparison of the equilibrium paths obtained for isotropic and kinematic strengthening for two example shell lengths is shown in Fig. 10. The differences between the obtained results are very small and become visible only in the late post-critical phase, but they exist, which means that there are small, local unloads in the calculated shells, despite monotonic nature of the load.

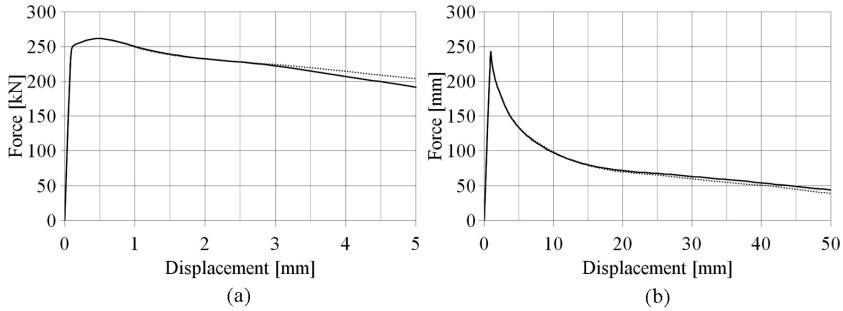

Fig. 10. Isotropic (solid) and kinematic (dotted) hardening: equilibrium paths for 50 mm (a) and 500 mm (b) long shell – material data according to Fig. 2a

6. Conclusions and summary

The compressed thin-walled perforated steel bars considered in this work are modeled as elastic-plastic shells, which requires the use of the finite element method, for which the ABAQUS program was used. The finite element mesh must be accurate, both due to the presence of holes with sharp corners and the expected concentrations and redistribution of plastic strains. The meshes used contain approximately 4000 elements in a repeatable 5 cm module. In order to determine the parameters of constitutive relations, 13 experimental uniaxial tensile tests were performed on samples cut from the considered bars. The theory of elasto-plasticity of large deformations available in the ABAQUS program with the Huber-Mises plasticity condition and isotropic and kinematic hardening with additive decomposition of the logarithmic strain tensor

into elastic and plastic parts was used. Among the nonlinear hardening description options available in the program, a uniaxial, piecewise-linear model was selected, based on data from a uniaxial tensile test.

Based on the results presented in this work, general and specific conclusions can be formulated. The most important is the need to model short thin-walled perforated bars as perforated shells and to apply the theory of elasto-plasticity of large deformations, which is also confirmed in studies on the design and analysis of metal structures [23, 24, 37], which include recommendations on the use the so-called geometrically and materially nonlinear theories.

The steel from which the bars are made is of low quality, and its properties vary by up to several dozen percent between individual, supposedly identical, elements. The most important parameters of the material model are the elastic modulus E, the yield stress R_{pl} and the tensile strength R_m. The same parameters were assumed in both the isotropic and kinematic hardening models. The value of the yield strength R_{pl} has the greatest decisive influence on the obtained load-bearing capacity values and the course of the equilibrium paths, because inelastic local or distortion buckling is dominant for short perforated bars. The value of the elastic modulus E mainly affects the equilibrium paths, especially in the pre-critical range. The value of tensile strength R_m is important only in the post-critical phase, with a higher value increasing the calculated force values, and a lower one decreasing them.

Differences between the results obtained for precisely and roughly approximated stress-plastic strain curves (piecewise linear approximation by specifying points on the curve) are noticeable both in the load-bearing capacity values (influence of several percent) and in the course of the equilibrium paths, especially in the post-critical phase, where more accurate approximation gives higher force values, and less accurate one – lower ones. Taking the proportional limit instead of the yield point as the beginning of yielding allows for obtaining a smoother course of the curve at the moment of buckling, closer to the experimental results; However, it should be recalled here that this approach only works in the case of monotonic loads – in the case of unloading, it is necessary to model non-linear elasticity between R_H and R_{pl}. It should also be noted that the choice of the type of hardening (isotropic or kinematic) does not affect the buckling and load-bearing capacity of the monotonically compressed shell (there are no local unloading before buckling) and becomes important only in the late post-critical phase, when, due to very large deformations and local rotations, local unloading occurs.

A high instability of the considered nonlinear boundary problem was noticed – the solution results are sensitive to the adopted parameters of the numerical algorithms. It happened that changes, e.g. in the step division, resulted in a change in the form of buckling and, as a result, the load-bearing capacity. This is due to the similar chance of the shell buckling inward or outward and the different buckling modes resulting from the initial direction of deformation. It is worth noting here that in the experimental tests, due to the boundary conditions and the occurrence of imperfections, the directions of buckling, and consequently also the values of critical forces, were much more stable. The analysis of the influence of boundary conditions and imperfections was presented in [18, 19, 26] – their significant impact on the calculated load capacity (up to several dozen percent) and buckling modes was found, and the adoption of imperfections and boundary conditions that well described the experimental conditions allowed for good compliance of experimental and numerical results.

References

[1] M. Prisco and M. Colombo, "FRC thin walled structures: opportunities and threats", in *8th RILEM International Symposium on Fiber Reinforced Concrete: challenges and opportunities (BEFIB 2012)*. RILEM Publications SARL, 2013, pp. 23–49.

[2] K. Falkowicz, "Stability analysis of thin-walled perforated composite columns using Finite Element Method", *Materials*, vol. 15, no. 24, art. no. 8919, 2022, doi: 10.3390/ma15248919.

[3] C. Ajdukiewicz and M. Gajewski, "Verification of the thin-walled beam theory with application of FEM and shell modelling", in *IOP Conference Series: Materials Science and Engineering*, vol. 661, 2019, doi: 10.1088/1757-899X/661/1/012005.

[4] J.B. Obrębski, *Cienkościenne sprężyste pręty proste*. Warsaw: Oficyna Wydawnicza Politechniki Warszawskiej, 1991.

[5] D.K. Pham, C.H. Pham, and G.J. Hancock, "Elastic buckling solution for perforated thin-walled channel sections in shear with an aspect ratio of 2.0", in *CIGOS 2019, Innovation for Sustainable Infrastructure. Lecture Notes in Civil Engineering*, vol. 54, C. Ha-Minh, et al., Eds. Singapore: Springer, 2020, pp. 275–280, doi: 10.1007/978-981-15-0802-8_41.

[6] A. Piotrowski, M. Gajewski, and C. Ajdukiewicz, "Application of digital image correlation system for analysis of local plastic instabilities of perforated thin-walled bars", in *MATEC Web of Conferences*, vol. 196, art. no. 1032, 2018, doi: 10.1051/matecconf/201819601032.

[7] Z. Yao and K. Rasmussen, "Finite Element modelling and parametric studies of perforated thin-walled steel columns", Research Report No. 948. University of Sydney, Faculty of Engineering, School of Civil Engineering, Sydney, Australia, 2014.

[8] Ł. Kowalewski, A. Piotrowski, M. Gajewski, and S. Jemioło, "FEM application for determination of post-critical deformation modes of perforated thin-walled bars", in *Monographs from Scientific Seminars Organized by Polish Chapters International Association for Shell and Spatial Structures*. Olsztyn: University of Warmia and Mazury, Faculty of Geodesy, Geospatial and Civil Engineering, 2016, pp. 27–30.

[9] Ł. Kowalewski, A. Piotrowski, M. Gajewski, and S. Jemioło, "Determination of critical forces with corresponding deformation modes for perforated thin-walled bars", in *Monographs from Scientific Seminars Organized by Polish Chapters International Association for Shell and Spatial Structures*. Bydgoszcz: University of Science and Technology, Faculty of Civil Engineering, Architecture and Environmental Engineering, 2017, pp. 14–17.

[10] A. Piotrowski, L. Kowalewski, R. Szczerba, M. Gajewski, and S. Jemiolo, "Buckling resistance assessment of thin-walled open section element under pure compression", *MATEC Web of Conferences*, vol. 86, art. no. 01021, 2016, doi: 10.1051/matecconf/20168601021.

[11] A. Piotrowski, "Weryfikacja modeli konstytutywnych sprężysto-plastyczności przy zastosowaniu MES i optycznej korelacji obrazu", PhD thesis, Warsaw University of Technology, Poland, 2023.

[12] P. Wysmulski, K. Falkowicz, and P. Filipek, "Buckling state analysis of compressed composite plates with cut-out", *Composite Structures*, vol. 274, art. no. 114345, 2021, doi: 10.1016/j.compstruct.2021.114345.

[13] T. da Silveira, J.P.S. Neufeld, L.A.O. Rocha, E.D. dos Santos, and L.A. Isoldi, "Numerical analysis of biaxial elasto-plastic buckling of perforated rectangular steel plates applying the Constructal Design method", *IOP Conference Series: Materials Science and Engineering*, vol. 1048, 2021, doi: 10.1088/1757-899X/1048/1/012017.

[14] M. Nedelcu, "Buckling mode identification of perforated thin-walled members by using GBT and shell FEA", *Thin-Walled Structures*, vol. 82, pp. 67–81, 2014, doi: 10.1016/j.tws.2014.04.005.

[15] K. Rzeszut, "Selected aspects of stability of thin-walled steel structures with clearences and initial imperfections", in *Lightweight Structures in Civil Engineering. Contemporary Problems. Local Seminar IASS Polish Chapters*, M. Kamiński, Ed. Łódź, 2018, pp. 119–125.

[16] V. Rybakov, Q. Ha, A. Gordeeva, and K. Urmanceva, "The stability of the thin-walled perforated compressed elements", in *Sustainable Energy Systems: Innovative Perspectives. SES 2020. Lecture Notes in Civil Engineering,* vol. 141, A. Sinitsyn, Ed. Cham: Springer, 2021, pp. 420–432, doi: 10.1007/978-3-030-67654-4_45.

[17] B. Salhab and Y. Wang, "An experimental study of perforated cold-formed thin-walled steel studs in fire", in *4th international conference on advances in steel structures (ICASS05), Tongji, China*. Tongji: 2005.

[18] A. Piotrowski, "Influence of imperfection on buckling resistance of perforated thin-walled bar with very low slenderness - FEM analysis and comparison with experimental results", *IOP Conference Series: Materials Science and Engineering*, vol. 661, 2019, doi: 10.1088/1757-899X/661/1/012003.

[19] A. Piotrowski and M. Gajewski, "Buckling resistance of short perforated thin-walled bars – FEM analysis and experimental results", in: *Theoretical foundation of civil engineering. Mechanics of materials and structures*, vol. 9, A. Szwed and I. Kamińska, Eds. Warsaw: Oficyna Wydawnicza Politechniki Warszawskiej, 2019, pp. 21–32.

[20] A. Piotrowski, M. Gajewski and C. Ajdukiewicz, "Local plastic instabilities of perforated thin-walled bars – FEM modelling and DIC verification", in *Materials Research Proceedings*, vol. 12, pp. 71–76, 2019, doi: 10.21741/9781644900215-10.

[21] A. Piotrowski, M. Gajewski, C. Ajdukiewicz, Ł. Kowalewski, and S. Jemioło, "Experimental and numerical determination of critical forces for perforated thin walled bars", in *Lightweight Structures in Civil Engineering. Contemporary Problems. Local Seminar IASS Polish Chapters*, M. Kamiński, Ed. Łódź, 2018, pp. 109–114.

[22] *ABAQUS/Standard User's manual, Version 6.11*. Dassault Systèmes, 2011.

[23] PN-EN 1993-1-1:2006 Eurocode 3: Design of steel structures: General rules and rules for buildings. PKN, 2006.

[24] L.S. da Silva, R.A.D. SimoÞes, and H. Gervaìsio, *Design of steel structures: Eurocode 3: Design of steel structures, part 1–1 – General rules and rules for buildings*. Brussels: ECCS, 2015, doi: 10.1002/9783433606483.

[25] W.W. Yu and R.A. LaBoube, *Cold-formed steel design,* 4^{th} ed. John Wiley & Sons, 2010, doi: 10.1002/9780470949825.

[26] A. Piotrowski, M. Gajewski, and C. Ajdukiewicz, "Experimental determination of critical forces for perforated thin walled bars in case of hinged support", in *Lightweight Structures in Civil Engineering Proceedings. 25th LSCE*, P. Bilko and L. Małyszko, Eds. Olsztyn: University of Warmia and Mazury, 2019.

[27] S. Jemioło and M. Gajewski, *Hipersprężystoplastyczność*. Warsaw: Oficyna Wydawnicza Politechniki Warszawskiej, 2014.

[28] E.A. de S. Neto, D. Pericì, and D.R.J. Owen, *Computational methods for plasticity: theory and applications*. Chichester, West Sussex, UK: John Wiley and Sons Ltd, 2008, doi: 10.1002/9780470694626.

[29] A.S. Khan and S. Huang, *Continuum theory of plasticity*. New York: Wiley, 1995.

[30] J. Lemaitre and J.L. Chaboche, *Mechanics of solid materials*. Cambridge University Press, 1990.

[31] J. Lubliner, *Plasticity Theory*. Mineola, NY, USA: Dover Publications, 2008.

[32] D. Hibbit, B. Karlsson, and P. Sorensen, *ABAQUS Theory manual, Version 6*. Pawtucket: Hibbitt, Karlsson and Sorensen, 2001.

[33] D. Hibbit, B. Karlsson, and P. Sorensen, *ABAQUS/Standard User's manual, Version 6*. Pawtucket: Hibbitt, Karlsson and Sorensen, 2001.

[34] Massachusetts Institute of Technology, "Defining plasticity in Abaqus". [Online]. Available: https://abaqus-docs.mit.edu/2017/English/SIMACAEGSARefMap/simagsa-c-matdefining.htm. [Accessed: 30 Nov. 2023].

[35] D. Hibbit, B. Karlsson, and P. Sorensen, *ABAQUS Verification manual, Version 6*. Pawtucket: Hibbitt, Karlsson and Sorensen, 2001.

[36] M. Gajewski, C. Ajdukiewicz, and A. Piotrowski, "Verification of plasticity theory with isotropic hardening and additive decomposition of left deformation tensor using digital image correlation system", *Solid State Phenomena*, vol. 240, pp. 61–66, 2016, doi: 10.4028/www.scientific.net/SSP.240.61.

[37] M. Giżejowski, R. Szczerba, M. Gajewski, and Z. Stachura, "On the resistance evaluation of lateral-torsional buckling of bisymmetrical I-section beams using Finite Element simulations", *Procedia Engineering*, vol. 153, pp. 180–188, 2016, doi: 10.1016/j.proeng.2016.08.100.

Wpływ dokładności odwzorowania jednoosiowej próby rozciągania stali miękkiej w modelu plastyczności H–M na zachowanie perforowanej cienkościennej powłoki poddanej ściskaniu

Słowa kluczowe: MES, nośność, sprężysto-plastyczność, stateczność, pręty cienkościenne, pręty perforowane

Streszczenie:

W artykule opisano wpływ modelowania relacji konstytutywnej plastyczności na wyboczenie poddanego ściskaniu krótkiego odcinka stalowego perforowanego pręta cienkościennego o przekroju otwartym (modelowanego jako perforowana powłoka) stanowiącego jeden z elementów systemu regałów wysokiego składowania. Wykonano obliczenia numeryczne w programie ABAQUS/Standard i wykorzystano zaimplementowaną w nim teorię sprężysto-plastyczności dużych deformacji z addytywną dekompozycją logarytmicznego tensora odkształcenia i nieliniowym wzmocnieniem izotropowym lub kinematycznym. Założono izotropowość materiału i przyjęto prawo płynięcia stowarzyszone z warunkiem plastyczności Hubera-Misesa. W zakresie sprężystym przyjęto liniową charakterystykę materiału, natomiast w zakresie plastycznym przebieg jednoosiowej krzywej wzmocnienia opisano odcinkowo na podstawie wykresów odkształcenie plastyczne – naprężenie otrzymanych z jednoosiowych prób rozciągania. Przeanalizowano 24 zestawy danych materiałowych otrzymanych na podstawie badań doświadczalnych i opisano wpływ różnic w wartościach stałych materiałowych (w testach przeprowadzonych na próbkach wyciętych z modelowanych prętów stwierdzono duże różnice w wartościach stałych materiałowych i charakterze wykresów rozciągania) oraz dokładności modelowania wzmocnienia (przyjętej liczbie odcinków w modelu odcinkowo liniowym) na obliczaną wartość nośności. Stal, z której wykonane są pręty, jest niskiej jakości, a jej właściwości różnią się nawet o kilkadziesiąt procent pomiędzy poszczególnymi, w założeniu identycznymi, elementami. Najważniejszymi parametrami modelu materiału są moduł sprężystości E, granica plastyczności R_{pl} oraz wytrzymałość na rozciąganie R_m. Te same parametry przyjęto zarówno w modelu ze wzmocnieniem izotropowym, jak i kinematycznym. Największy, decydujący wpływ na otrzymane wartości nośności i przebieg ścieżek równowagi ma wartość granicy plastyczności R_{pl}, gdyż dla krótkich prętów perforowanych dominujące jest niesprężyste wyboczenie lokalne lub dystorsyjne. Wartość modułu sprężystości E wpływa głównie na ścieżki równowagi, przede wszystkim w zakresie przedkrytycznym. Wartość wytrzymałości na rozciąganie R_m ma znaczenie dopiero w fazie postkrytycznej, przy czym większa jej wartość zwiększa obliczane wartości sił, a mniejsza je zmniejsza. Różnice między wynikami otrzymanymi dla dokładnie i zgrubnie odwzorowanych krzywych naprężenie – odkształcenie plastyczne (odwzorowanie odcinkowo liniowe przez podanie punktów na krzywej) są zauważalne zarówno w wartościach nośności (wpływ rzędu kilku procent) jak i w przebiegu ścieżek równowagi, przede wszystkim w fazie postkrytycznej, gdzie dokładniejsze odwzorowanie daje większe wartości sił, a mniej dokładne – mniejsze. Przyjęcie jako początku uplastycznienia granicy proporcjonalności zamiast granicy plastyczności pozwala na otrzymanie łagodniejszego, bliższego wynikom doświadczalnym, przebiegu krzywej w chwili wyboczenia; należy tu jednak przypomnieć, że jest to podejście sprawdzające się wyłącznie w przypadku obciążeń monotonicznych – w przypadku odciążeń konieczne jest modelowanie między R_H i R_{pl} nieliniowej sprężystości. Zauważyć również należy, że wybór rodzaju wzmocnienia (izotropowe lub kinematyczne) nie wpływa na wyboczenie i nośność monotonicznie ściskanej powłoki (nie ma lokalnych odciążeń przed wyboczeniem) i zaczyna odgrywać znaczenie dopiero w późnej fazie postkrytycznej, kiedy na skutek bardzo dużych deformacji i lokalnych obrotów pojawiają się miejscowe odciążenia. Zauważono dużą niestabilność rozpatrywanego nieliniowego zadania brzegowego – wyniki rozwiązania są wrażliwe na przyjęte parametry algorytmów numerycznych. Zdarzało się, że zmiany np. w podziale

kroku skutkowały zmianą postaci wyboczenia i w efekcie nośności. Jest to spowodowane zbliżoną szansą na wyboczenie powłoki do środka lub na zewnątrz i odmiennością wynikających z początkowego kierunku deformacji postaci wyboczenia. Warto tutaj zauważyć, że w badaniach doświadczalnych, z uwagi na warunki brzegowe oraz występowanie imperfekcji, kierunki wyboczenia, a w rezultacie również wartości sił krytycznych, były zdecydowanie bardziej stabilne. Analizę wpływu warunków brzegowych oraz imperfekcji zaprezentowano we wcześniejszych pracach; stwierdzono ich znaczny wpływ na obliczaną nośność (nawet do kilkudziesięciu procent) i postacie wyboczenia, przy czym przyjęcie imperfekcji i warunków brzegowych dobrze opisujących warunki doświadczenia pozwalało uzyskać dobrą zgodność wyników doświadczalnych z obliczeniowymi. Najważniejszym wnioskiem o charakterze ogólnym wypływającym z przedstawionych w niniejszej pracy wyników jest konieczność modelowania krótkich cienkościennych prętów perforowanych jako perforowanych powłok oraz zastosowania teorii sprężysto-plastyczności dużych deformacji, co potwierdzone jest także w opracowaniach dotyczących projektowania i analizy konstrukcji metalowych, gdzie znajdują się zalecenia o stosowaniu tzw. teorii geometrycznie i materiałowo nieliniowych.

Received: 2024-05-09, Revised: 2024-05-28